Structural and electrochemical performance of three-dimensional LiMn$_2$O$_4$ thin film

**Bo Gun Park · Soohyun Kim · Il-Doo Kim ·
Yong Joon Park**

Abstract LiMn$_2$O$_4$ thin films with three-dimensional (3D) structure were prepared by the sol–gel method. Polystyrene beads (300 nm) were dispersed in the form of monolayers on Pt/Ti/SiO$_2$/Si substrates, which were then used as templates for fabricating three-dimensionally ordered electrodes. A coating solution prepared from acetylacetonate sources was dropped on the template-deposited substrates, which were then calcinated at 400 °C. The templates were removed by calcinations, and a 3D structure was formed through an annealing process. The discharge capacity of the 3D LiMn$_2$O$_4$ films was 1.63–3.03 μAh cm^{-2}. The capacity loss over 100 cycles was approximately 18%, however, the 3D structure was not destroyed during cycling.

Introduction

Though microelectromechanical system (MEMS) devices have developed tremendously over the last decade, the need for small-scale power sources has not been successfully met, and their development remains one of the challenges to be overcome in the continuing trend toward miniaturization. In the case of small-scale batteries, the achievable power and energy densities do not scale down favorably because packaging and the internal battery hardware determine their overall size and mass to a large extent. Of the several approaches that have been examined thus far, thin-film batteries have been one of the most promising technologies for solving this problem [1–4].

In recent years, it has been realized that the performance of thin-film batteries can be improved by reconfiguring the electrode materials currently employed in two-dimensional (2D) batteries into three-dimensional (3D) architectures [1–11]. Figure 1 shows a comparison of a 2D with a 3D electrode. In 2D design, if the electrode thickness is increased to obtain high capacity, it will lead to an increase in the electrode length (L) and the diffusion distance of lithium ions for the charge–discharge reaction. As a result, thin-film batteries with thick electrodes are very susceptible to ohmic losses and other transport limitations. However, in 3D thin-film batteries, an increase in the electrode thickness does not cause an increase in the diffusion distance of lithium ions [1, 12–16]. This structural feature facilitates the fabrication of large-capacity thin-film batteries by increasing the electrode thickness without imposing a transport limitation on lithium ions. Further, it is clear that the 3D structure of electrodes offers them improved charge–discharge kinetics owing to their large surface area for Faradaic reactions, in addition to offering the added freedom for a volume change that accompanies lithium–ion intercalation and deintercalation.

One of the most critical processes for 3D battery design is the fabrication of an electrode material with a periodically ordered macro-porous structure. The open volume of
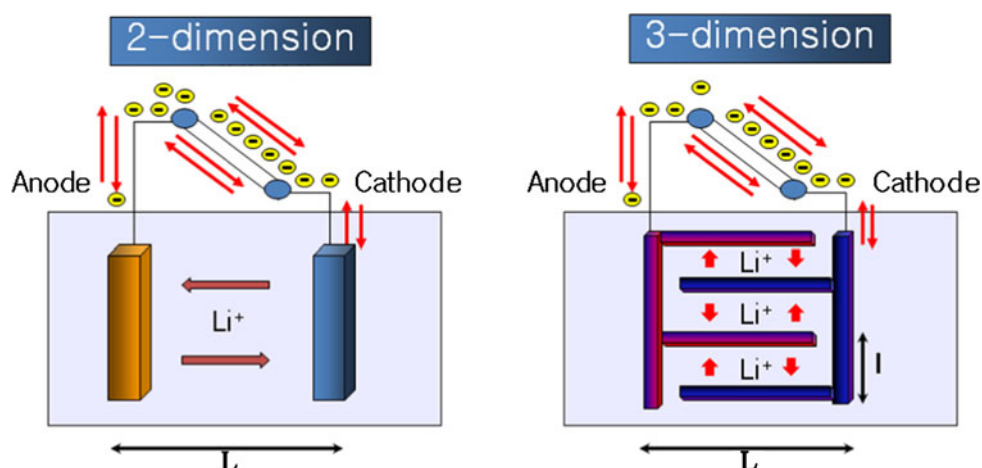
B. G. Park · Y. J. Park (✉)
Department of Advanced Materials Engineering, Kyonggi
University, San 94-6, Yiui-dong, Yeongtong-gu, Suwon,
Gyeonggi-do 443-760, Republic of Korea
e-mail: yjpark2006@kyonggi.ac.kr

S. Kim
Center for Energy Materials Research, Korea Institute of Science
and Technology, Seoul 130-650, Republic of Korea

S. Kim
Department of Chemical and Biological Engineering, Seoul
National University, Seoul 151-744, Republic of Korea

I.-D. Kim
Optoelectronic Materials Research Center, Korea Institute
of Science and Technology, Seoul 130-650, Republic of Korea

Fig. 1 Comparison of the charge–discharge processes of electrodes with 2D and 3D structures

such a macro-porous structure can be filled with a second phase, for example, an infiltrated electrolyte or even an opposing electrode structure may be filled in, thereby forming a true 3D battery assembly. Herein, $LiMn_2O_4$ thin film with three-dimensionally ordered macro-porous structure was prepared as a cathode for use in a 3D thin-film battery. Various deposition techniques such as chemical vapor deposition (CVD) [17, 18], radio frequency (RF) sputtering [19, 20], pulsed laser deposition (PLD) [21, 22], ink-jet printing [23], and the sol–gel method [24, 25] have so far been used to fabricate thin-film electrodes. In this study, the sol–gel method was used to prepare a $LiMn_2O_4$ thin film and, polystyrene microsphere beads were used as a template to form the 3D structure. The electrochemical and structural properties of the resulting 3D $LiMn_2O_4$ electrodes were investigated using a battery cycler, scanning electron microscopy (SEM), and X-ray diffraction (XRD).

Experimental

A polystyrene template was used to develop an ordered macro-porous network for fabricating the electrodes. An aqueous suspension (1 wt%) of polystyrene microspheres (300 nm) was ultrasonically dispersed in deionized water, and the microspheres were coated and dried on $Pt/Ti/SiO_2/Si$ substrates by the dip coating method. The sol for thin-film deposition was made by mixing precursors and solvents. The precursor materials were manganese (III) acetylacetonate [$Mn(CH_3CO\text{-}CHCOCH_3)_3$] and lithium acetylacetonate [$LiCH_3CO\text{-}CHCOCH_3$]. Each precursor concentration was controlled to adjust the ratio Li:Mn = 1:2. Further, 1-butanol and acetic acid were used as solvents. The precursor solution (0.4 M) was stirred using a magnetic stirrer for 10 h, and passed through a 0.2-μm filter prior to use. Subsequently, by means of a pipet, it was dripped onto the template-deposited substrates and dried at

room temperature. The deposited films were calcinated at 400 °C for 30 min to remove the polystyrene template and the organic materials of the precursors. The film samples were then annealed at 700, 750, and 800 °C for 10 min using a rapid thermal annealing (RTA) system in an air atmosphere for crystallization. Figure 2 shows a schematic diagram of the fabrication process of the 3D $LiMn_2O_4$ thin-film electrodes.

The thermal decomposition behavior of the polystyrene template was examined by differential scanning calorimeter (DSC) analysis. The heating rate and the temperature range of the DSC tests were 5 °C/min and 25–500 °C,
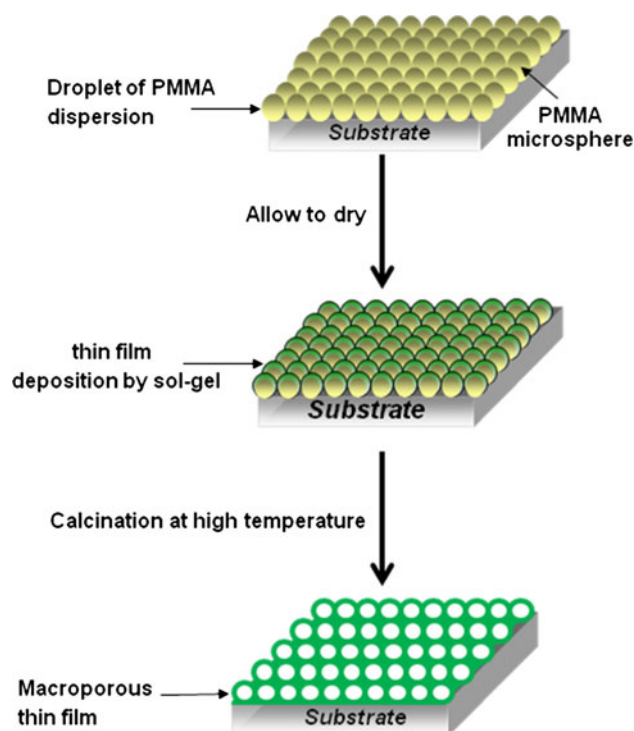

Fig. 2 Schematic diagram of the fabrication process of 3D $LiMn_2O_4$ thin-film electrodes

respectively. The phases present in the $LiMn_2O_4$ thin films were analyzed using an X-ray diffractometer (Philips) with monochromatized Cu Kα radiation ($\lambda = 1.5406$ Å). The film morphology was observed by FE-SEM. For electrochemical measurements, a $LiMn_2O_4$ thin film was placed in a beaker cell containing 1 M $LiClO_4$ in propylene carbonate (PC), and a lithium foil counter electrode, which was prepared in an Ar-atmosphere glove box. Charge–discharge tests were controlled with a galvanostatic test system (Wonatech).
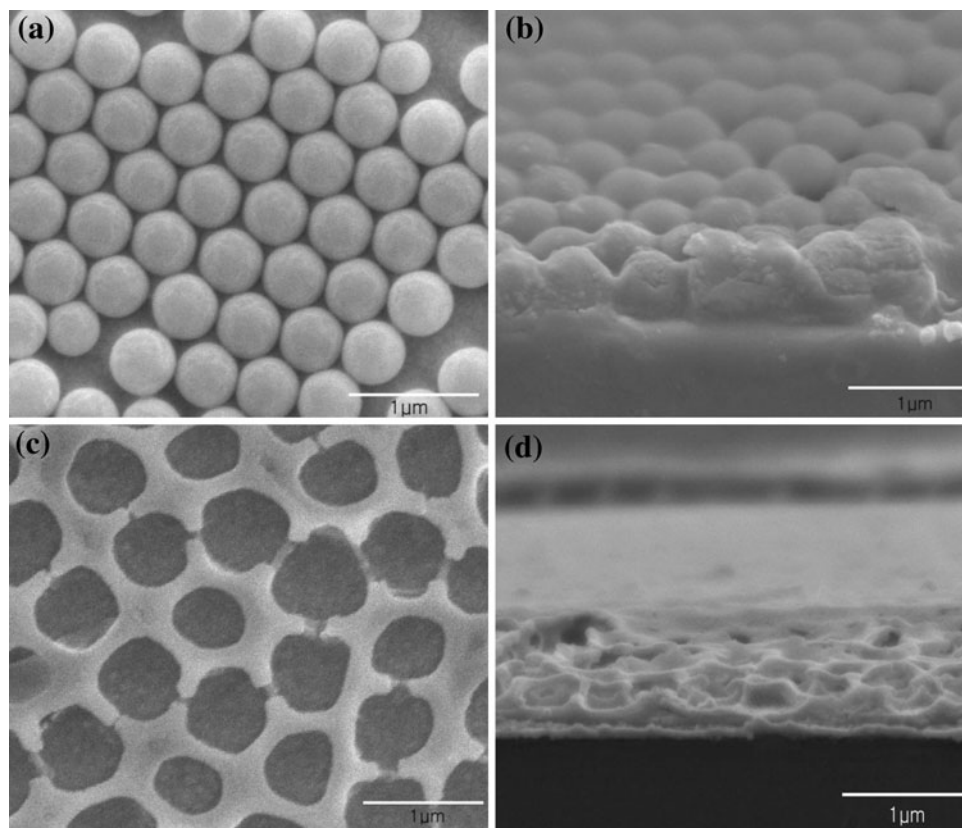
Results and discussion

FE-SEM images of an as-deposited polystyrene template are shown in Fig. 3a. The figure shows that the template was successfully coated as a monolayer on the substrate, which is important for fabricating a uniform three-dimensional thin-film electrode. If the polystyrene beads had been deposited as a multilayer, the open volume formed from the template would have been connected in a zig-zag manner rather than perpendicularly. This would have made it difficult to fill the open volume with an electrolyte and thus form the opposite electrode for a truly 3D thin-film battery. Further, the polystyrene beads were attached with a close-packed hexagonal structure on the surface of the substrate.

The template layer exhibited sufficiently good adhesion for the subsequent permeation of the precursor solution. In the image of the template film coated by the precursor solution (Fig. 3b), the 3D architecture seems to have remained unchanged after the deposition of the Li–Mn–O film.

The thermal decomposition behavior of the polystyrene beads was examined by differential scanning calorimeter (DSC) analysis. As shown in Fig. 4, the main heat flow decreased between 240 and 380 °C due to the calcination of the polystyrene beads. Thereafter, no thermal reaction was detected, indicating the perfect removal of the polystyrene template. In line with the DSC results, 400 °C was selected as the calcinations temperature for removing the polystyrene beads. Figure 3c and d display the FE-SEM images of the 3D thin film after the film was calcined at 400 °C for removing the template and organic precursor materials. It is confirmed that uniform voids were formed on the film due to the removal of the template, although the small holes were partially occupied without complete alignment. The mean size of the uniform voids, measured from the images, ranges from 0.3 to 0.5 μm. The spherical voids of the inverse-opal geometry form a 3D structure. The interconnected wall structure of this formation can provide a continuous electronic conduction and diffusion pathway for lithium ions. Moreover, the high volume of

Fig. 3 FE-SEM images of template-deposited substrate. **a** Top view and **b** cross-sectional image after coating the substrate with precursor solution. FE-SEM images of 3D Li–Mn–O precursor film after calcination at 400 °C for 30 min. **c** Top view and **d** cross-sectional image
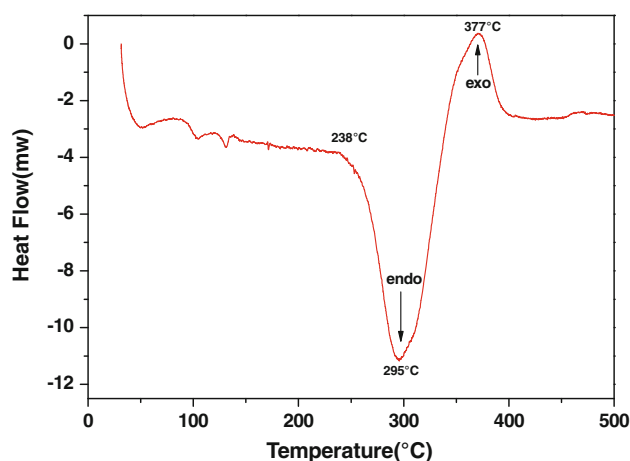
Fig. 4 DSC profile of polystyrene beads

Fig. 5 XRD patterns of 3D $LiMn_2O_4$ thin films. (*a*) Film calcinated at 400 °C for 30 min, (*b*) film annealed at 700 °C for 10 min after calcinations, (*c*) film annealed at 750 °C for 10 min after calcinations, and (*d*) film annealed at 800 °C for 10 min after calcination

surface area of the 3D electrode is readily and uniformly accessible to the electrolyte, which facilitates lithium–ion diffusion during charge–discharge reactions. In a 2D thin-film battery, an increase in the film thickness implies an increase in the diffusion length of lithium ions. In addition, thin-film electrodes do not contain conducting agents such as carbon, and a thick electrode film will increase the ohmic resistance of the film electrode. Therefore, if the thickness of a film electrode is increased to obtain a large discharge capacity, then the rate capability and discharge capacity of the thin-film battery deteriorate due to a long diffusion length of lithium ions and high ohmic resistance. However, in 3D thin-film batteries, the thickness of the electrode film is not directly associated with the diffusion length of lithium ions and electrons. As explained in Fig. 1, the thickness of a film electrode can be increased to obtain a high-capacity battery without sacrificing the rate capability.

The phases present in the 3D $LiMn_2O_4$ thin films were investigated through XRD analysis after annealing the films. Figure 5a shows the XRD patterns of the precursor film calcinated at 400 °C for 30 min. without performing the annealing process. In these patterns, no diffraction peaks were detected, except for those of Pt and Si. However, it is possible that the peak related with (311) diffraction was overlapped with substrate peak. The background level of the detected peaks was not significantly high, indicating that the residual organic materials formed from the precursors or the polystyrene template was almost completely removed during calcination. The film samples were annealed for crystallization at 700 °C for 10 min, 750 °C for 10 min, and 800 °C for 10 min in an air atmosphere, using RTA. As shown in Fig. 5b–d, several diffraction peaks appeared, indicating crystallization during the annealing process. The peaks located at $2\theta = 18.64°$, 36.13°, and 44.10° correspond to the (111), (311), and
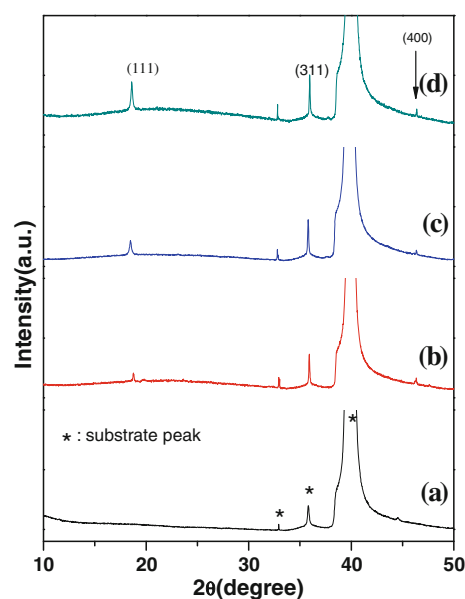
(400) diffraction reflections of a typical spinel $LiMn_2O_4$ lattice (JCPDS 89-0118), respectively. The observed peaks became sharper, i.e., the crystallinity of the film seems to improve as well as the increase of crystallite size, with an increase in the annealing temperature.

Figure 6 displays the FE-SEM images of the $LiMn_2O_4$ thin-film samples annealed at 700, 750, and 800 °C for 10 min. The film samples maintained a 3D networks with interconnected porosity after annealing. The sample annealed at 700 °C exhibited a shape similar to that of the sample calcinated at 400 °C. Its pores were highly ordered, with a diameter of approximately 0.3–0.5 μm, and the thickness of pores walls was less than 0.1 μm. However, as annealing temperature increased (750 or 800 °C), breaks appeared in the walls of the network, and several pores seemed to shrink at various locations on the $LiMn_2O_4$ thin film. This is possibly due to the shrinkage of the $LiMn_2O_4$ film because of the sintering effect that occurs during the annealing process at higher temperatures. This suggests that controlling the annealing temperature is an important factor for sustaining the stability of the 3D network of the film. Further, no serious deterioration of the adhesion between the film and the substrate was observed.

Figure 7 shows the discharge curves of the 3D $LiMn_2O_4$ thin-film electrodes annealed at 700 °C for 10 min, 750 °C for 10 min, and 800 °C for 10 min. These curves were measured with a current density of 100 nAh cm^{-2} in the voltage range of 4.3–3.7 V. The initial discharge capacities were 1.63, 2.34, and 3.03 μAh cm^{-2} for the samples annealed for 10 min at temperatures of 700, 750, and
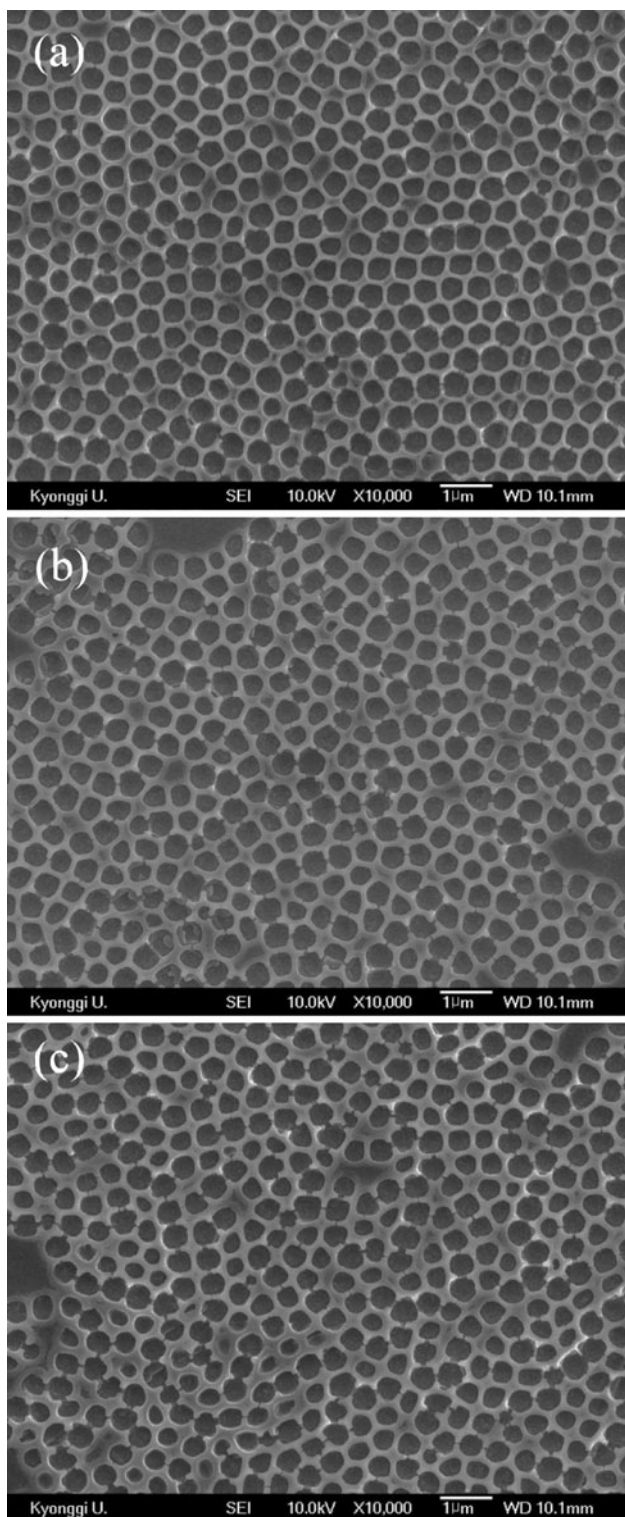
Fig. 6 FE-SEM images of 3D LiMn₂O₄ thin-films. **a** Film annealed at 700 °C for 10 min, **b** film annealed at 750 °C for 10 min, and **c** film annealed at 800 °C for 10 min

Fig. 7 Discharge profiles of 3D LiMn₂O₄ thin-film electrodes (current density = 100 nAh cm⁻²). **a** Film annealed at 700 °C for 10 min, **b** film annealed at 750 °C for 10 min, and **c** film annealed at 800 °C for 10 min

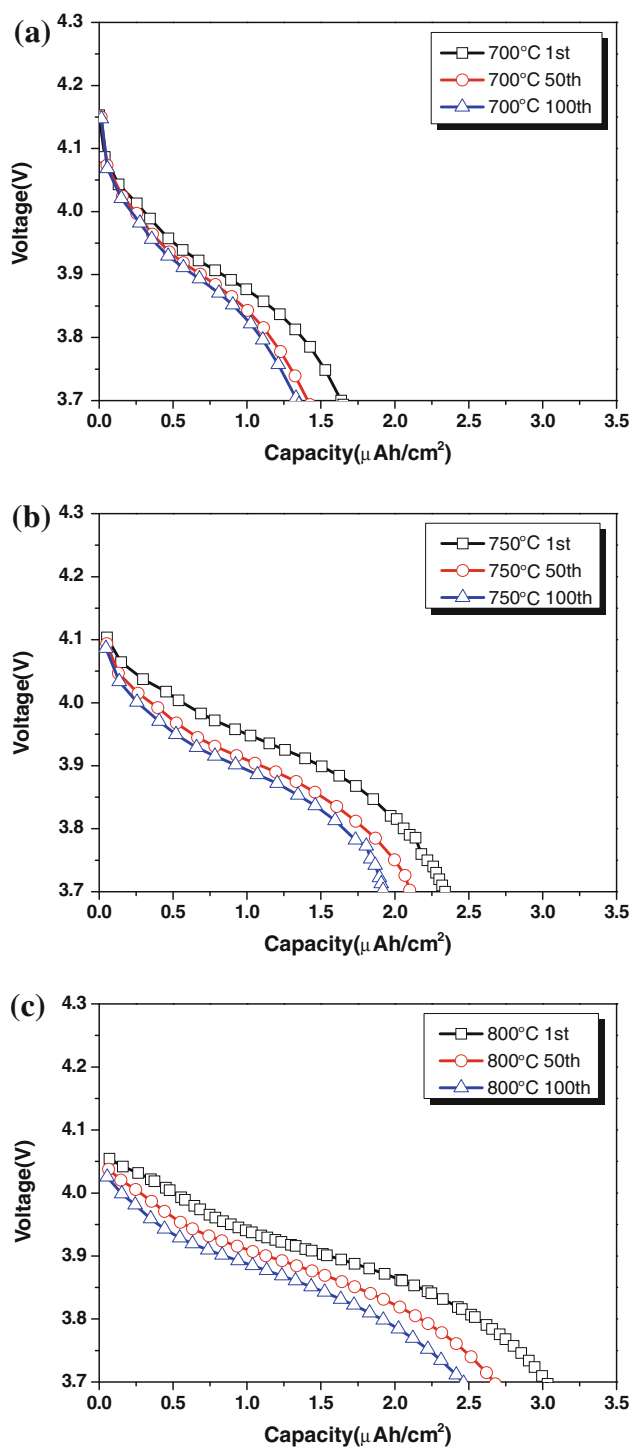800 °C, respectively. The higher the annealing temperature, the higher the initial discharge capacity of the 3D LiMn₂O₄ thin film is. This is due to the relatively superior crystallinity of the thin film annealed at a high temperature. The theoretical capacity of a 2D thin film of LiMn₂O₄ is 63 μAh cm⁻² μm⁻¹, if the density of the film is the same with the bulk one (4.28 g cm⁻³). However, actually the

density of the film was lower than the bulk one, the real capacity of $LiMn_2O_4$ film prepared by sol–gel method was 30–40 $\mu Ah\ cm^{-2}\ \mu m^{-1}$ [24, 25]. Based on this, the amount of active material of 3D $LiMn_2O_4$ thin film seems to be similar with the 3D $LiMn_2O_4$ thin film with thickness of 20 nm.

In general, the discharge profile of a $LiMn_2O_4$ thin film is divided into two voltage plateaus at about 4 V. However, the 3D $LiMn_2O_4$ thin-film electrodes studied here did not exhibit two clear voltage plateaus. It is possible that an increase in the annealing time or temperature led to an enhancement in crystallinity and discharge capacity. However, the 3D structure seems to be too unstable to sustain a much higher temperature. In a previous study [26], a film was annealed in a furnace system at 800 °C for 1 h to obtain a $LiMn_2O_4$ thin film with good crystallinity. However, some sections of the film began to peel from the substrate due to the shrinkage of the film. The 3D architecture of the film seems to be so delicate that carefully controlling the heating conditions is necessary to a prepare film with a stable structure. In this study, considering the discharge capacity, the sample annealed at 800 °C seems to be good. However, the sample annealed at 750 °C seems to be better, if we would like to obtain more stable 3D architecture. The discharge capacity of the 3D electrodes somewhat decreased with increased cycling. The cyclic performance of the 3D $LiMn_2O_4$ thin-film electrodes over 100 cycles is displayed in Fig. 8. The capacity retention of all the samples was about 82% after 100 cycles. Although a small capacity loss occurred, the 3D structure was preserved during cycling. Moreover, the adhesion of the 3D film did not suffer deterioration due to the charge–discharge process.
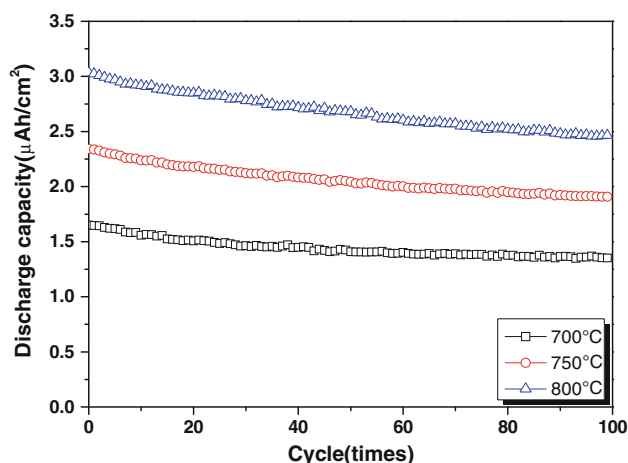

Fig. 8 Cyclic performance of 3D $LiMn_2O_4$ thin film electrodes

Conclusion

3D $LiMn_2O_4$ thin-film electrodes were fabricated by the sol–gel method on $Pt/Ti/SiO_2/Si$ substrates. Polystyrene microspheres were used as a template to develop the ordered macro-porous network for fabricating the electrodes. On removing the template from a deposited film, spherical voids of inverse-opal geometry were formed on the film, shaping the 3D structure of the $LiMn_2O_4$ film. The interconnected wall structure of the film can provide a continuous electronic conduction and diffusion pathway for lithium ions. The 3D electrodes annealed at 700 °C for 10 min, 750 °C for 10 min, and 800 °C for 10 min showed discharge capacities of 1.63, 2.34, and 3.03 $\mu Ah\ cm^{-2}$, respectively. The capacity retention of the film was about 82% for 100 cycles and the 3D structure was preserved during cycling.

References

1. Long JW, Dunn B, Rolison DR, White HS (2004) Chem Rev 104:4463
2. Nishizawa M, Mukai K, Kuwabata S, Martin CR, Yoneyama H (1997) J Electrochem Soc 144:1923
3. Teixidor GT, Zaouk RB, Park BY, Madou MJ (2008) J Power Source 183:730
4. Bates JB, Dudney NJ, Neudecker B, Ueda A, Evans CD (2000) Solid State Ionics 135:33
5. Ergang NS, Fierke MA, Wang Z, Smyrl WH, Stein A (2007) J Electrochem Soc 154:A1135
6. Albano F, Lin YS, Blaauw D, Sylvester DM, Wise KD, Sastry AM (2008) J Power Source 185:1524
7. Tonti D, Torralvo MJ, Ensiso E, Sobrados I, Sanz J (2008) Chem Mater 20:4783
8. Lee KT, Lytle JC, Eragang NS, Oh SM, Stein A (2005) Adv Funct Mater 15:547
9. Son JT, Park KS, Kim HG (2004) J Mater Sci 39:3635. doi: 10.1023/B:JMSC.0000030716.52790.96
10. Callone E, Fletcher JM, Carturan G, Raj R (2008) J Mater Sci 43:4862. doi:10.1007/s10853-008-2707-x
11. Wang D, Ding N, Song XH, Chen CH (2009) J Mater Sci 44:198. doi:10.1007/s10853-008-3104-1
12. Lee JT, Chu YJ, Wang FM, Yang CR, Li CC (2007) J Mater Sci 42:10118. doi:10.1007/s10853-007-2068-x
13. Yi TF, Hu XG, Dai CS, Gao K (2007) J Mater Sci 42:3825. doi: 10.1007/s10853-006-0460-6
14. Wu MS, Lee JT, Chiang PCJ, Lin JC (2007) J Mater Sci 42:259. doi:10.1007/s10853-006-1062-z
15. Sorek Y, Zhou P, Fischer E, Ishihara T (2000) J Mater Sci 35:4337. doi:10.1023/A:1004896621411
16. Fu YP, Su YH, Lin CH, Wu SH (2006) J Mater Sci 41:1157. doi: 10.1007/s10853-005-3646-4
17. Che G, Jirage KB, Fisher ER, Martin CR (1997) J Electrochem Soc 144:4296

18. Frangaud P, Nagarajan R, Schleich DM, Vujic D (1995) J Power Sources 54:362
19. Chiu KF (2007) Thin Solid Films 515:4614
20. Moon HS, Lee W, Reucroft PJ, Park JW (2003) J Power Sources 119–121:710
21. Otsuji H, Kawahara K, Ikegami T, Ebihara K (2006) Thin Solid Films 506–507:120
22. Xie J, Kohno K, Matsumura T, Imanishi N, Hirano A, Takeda Y, Yamamoto O (2008) Electrochim Acta 54:376
23. Huang J, Yang J, Li W, Cai W, Jiang Z (2008) Thin Solid Films 516:3314
24. Park YJ, Kim JG, Chung HT, Um WS, Kim MH, Kim HG (1998) J Power Source 76:41
25. Park YJ, Kim JG, Kim MK, Chang HT, Kim HG (2000) Solid State Ionics 130:203
26. Park BG, Ryu JH, Choi WY, Park YJ (2009) Bull Korean Chem Soc 30:653